

# A NOVEL 3D CONNECTOR-BEAM LATTICE MODEL: FROM MICROMORPHOLOGY TO MACROSCOPIC BEHAVIOR OF WOOD

EMI Conference 2022  
Baltimore, MD  
June 01, 2022

Hao Yin, Erol Lale, Eric Landis, and Gianluca Cusatis

# Outline

- Introduction
- Connector-Beam Lattice Model for Wood
  - Wood Micromorphology
  - Connector-Beam Lattice Model Formulation
  - Wood Test Simulations
- Conclusions and Future Work



# Introduction

- Wood, due to its low CO<sub>2</sub> and energy content relative to structural properties, as well as the innovations in engineered wood products, is at a new high of interest in construction engineering.
- However, design and code approval of new wood products still rely on expensive, time-consuming broad-based laboratory testing.



Figure 1: Brocks Commons tallwood house <sup>[1]</sup>

# Discrete modeling at finer scales: a powerful tool

- While many continuum-based, macroscale models have been successfully developed to represent the damage or failure of wood occurred at larger length scales, the discrete, finer scale modeling techniques, are also crucially important for capturing the intrinsic anisotropy and heterogeneity of wood.

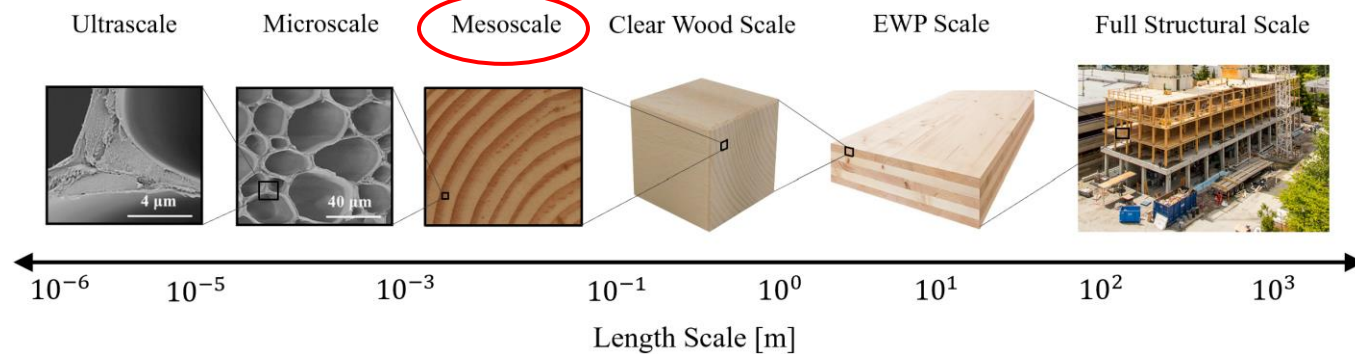


Figure 2: Various length scales of wood

# Connector-Beam Lattice Model for Wood

- A 3D discrete Connector-Beam Lattice (CBL) model has been developed, for explicitly simulating many mechanical behaviors (e.g., fracture) of wood at the mesoscale.

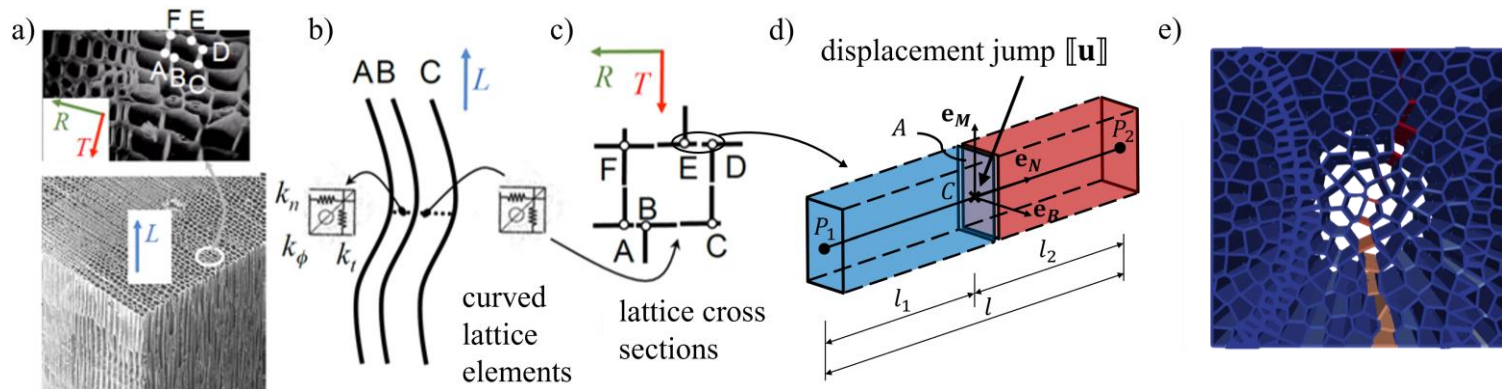


Figure 3: a) 3D morphology of wood mesostructure, b) curved axes of beam lattices, c) cross-sections of beam lattices, d) schematic diagram of the connector element, and e) Voronoi-based CBL model for wood

# Wood mesh generation

- The morphological structure of wood is one of the key aspects of the *CBL model*, as it may strongly affect both the elastic and fracture properties.
- We developed a Voronoi diagrams-based geometric generation tool that generates 3D meshes and models for wood.

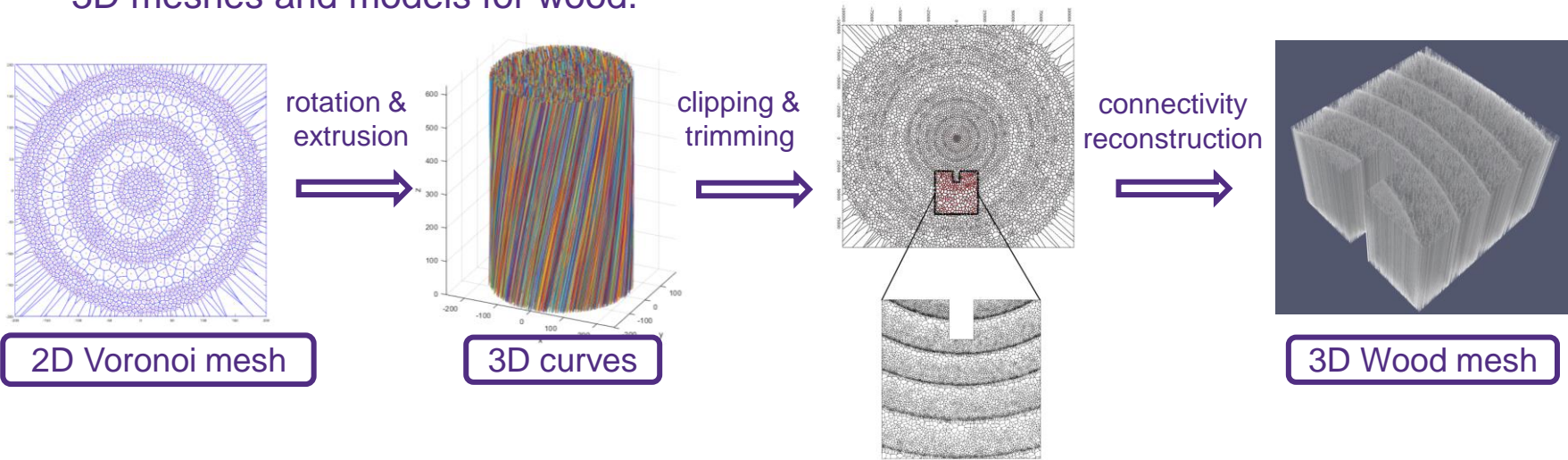


Figure 4: Workflow of wood mesh generation

# Wood mesh generation: annual rings

- The formulation of the annual rings follows density models of annual rings (by now, Pernestål et al., 1995).

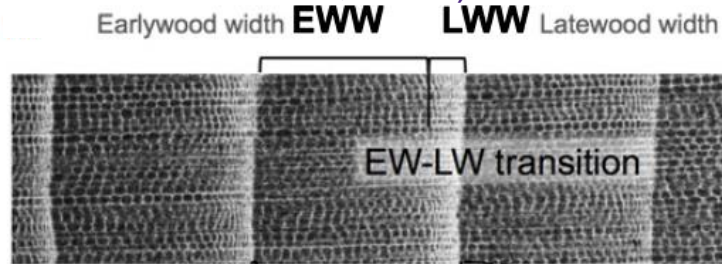


Figure 5: Earlywood-latewood transition [2]

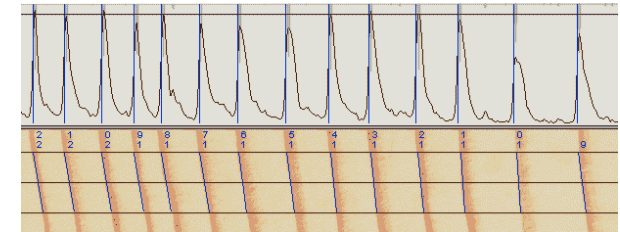


Figure 6: Density model of annual rings [3]

HWW = heartwood width  
EWW = earlywood width  
LWW = latewood width

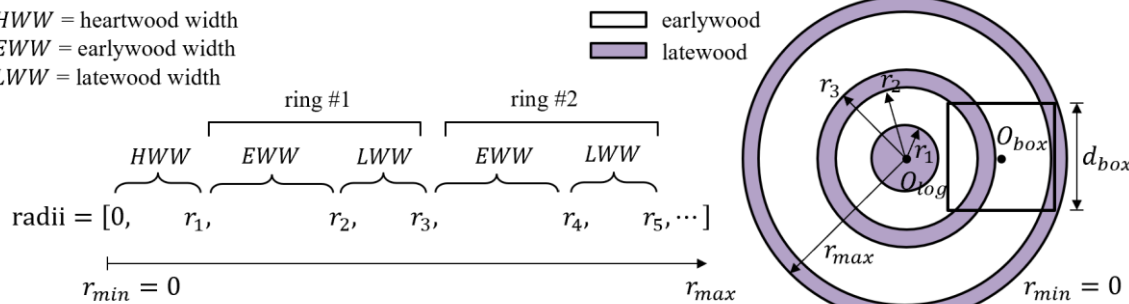


Figure 7: Annual rings structure in wood mesh

[2] Credit: Pernestål, K., B. Jonsson, and B. Larsson. "A simple model for density of annual rings." *Wood Science and Technology* 29.6 (1995): 441-449.

[3] Credit: [https://regentinstruments.com/assets/images\\_windendro/StraightPath\\_610.fw.png](https://regentinstruments.com/assets/images_windendro/StraightPath_610.fw.png)

# Wood mesh generation: clipping & trimming

- The 2D Voronoi diagram is formed and extruded in the out-of-plane (longitudinal) direction. Then cells intersect with the bounding box are clipped & trimmed.

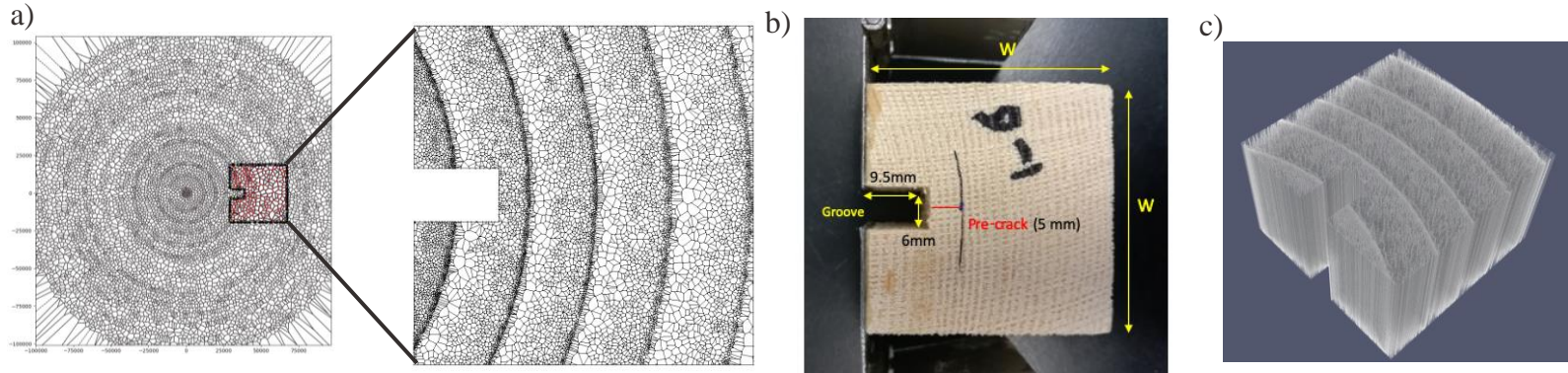


Figure 8: Wood mesh generation for a notched sample: a) the clipping and trimming algorithm b) a wood notched test sample (By courtesy of Belalpour and Landis), c) the corresponding wood mesh

# Wood mesh generation: visualization

- The data structure of wood mesh is reconstructed to have the connector-beam connectivities.

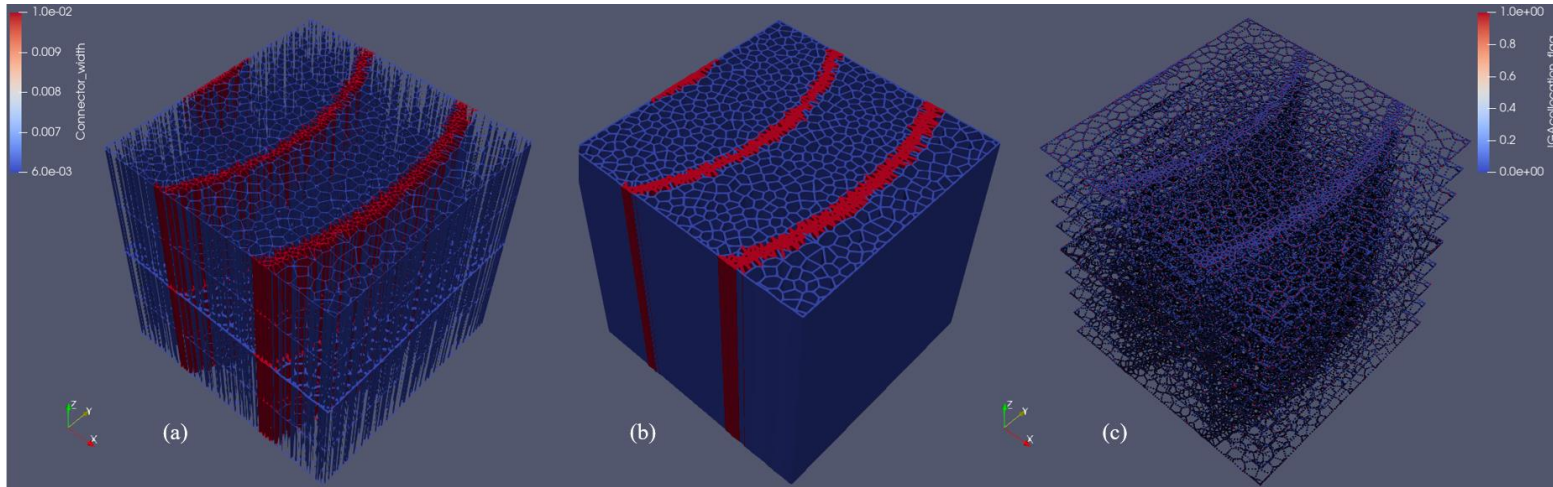


Figure 9: Visualization of a wood mesh: (a) connector-beam system, (b) volumetric rendering of connectors and beams, (c) point cloud of vertices (nodes)

now on *Github* as a *Python* package “*RingsPy*”

# Isogeometric beam lattice

- For the beam lattices, 3D curved Timoshenko beams with cruciform cross-sections are used.

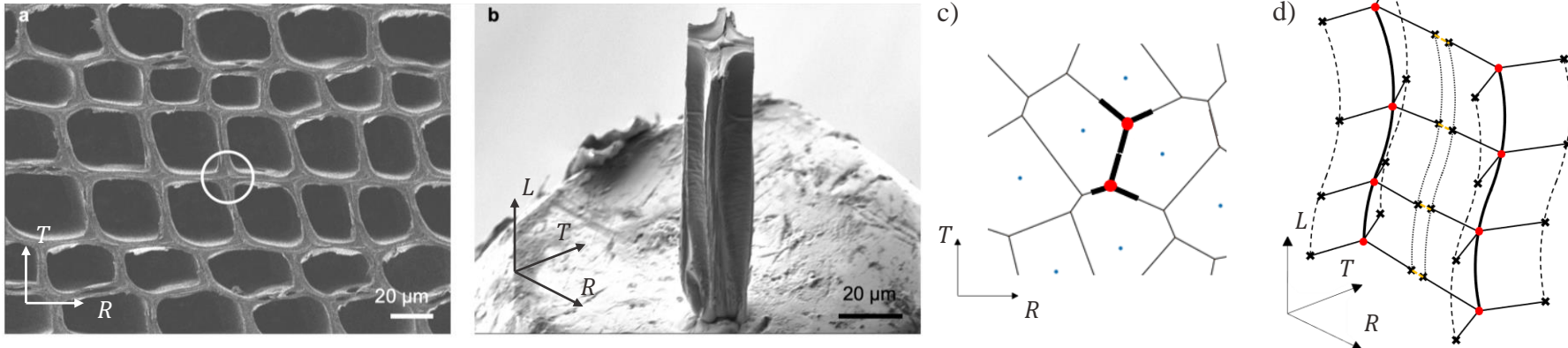


Figure 10: a) Cross-sectional view of wood cells, b) a single wood fiber specimen made by focused ion beam (FIB) milling, c) cross-sectional view of the virtual wood mesh, and d) 3D sketch of beam lattices (a and b are modified from [4])

# Isogeometric beam lattice

- The formulation of the beam lattice was derived [5].

Assumptions: (i) beam axis  $\perp$  section (ii) plane section (iii) small  $\mathbf{u}$  and  $\theta$

Kinematics:  $\mathbf{u} = \mathbf{u}_0 + \theta \times \mathbf{p}$

Jacobian from Cartesian system to curvilinear system

Compatibility:  $\boldsymbol{\epsilon} = (\nabla_X \mathbf{u} + \nabla_X \mathbf{u}^T)/2 \quad \nabla_X \mathbf{u} = \nabla_t \mathbf{u} \cdot \mathbf{J}^{-1}$

Non-zero components of  $\boldsymbol{\epsilon}$ :

$$\varepsilon_{tt} = \mathbf{t}^T \cdot \boldsymbol{\epsilon} \cdot \mathbf{t} \quad \gamma_{tn} = \mathbf{n}^T \cdot \boldsymbol{\epsilon} \cdot \mathbf{t} + \mathbf{t}^T \cdot \boldsymbol{\epsilon} \cdot \mathbf{n} \quad \gamma_{tb} = \mathbf{b}^T \cdot \boldsymbol{\epsilon} \cdot \mathbf{t} + \mathbf{t}^T \cdot \boldsymbol{\epsilon} \cdot \mathbf{b}$$

Equilibrium (through the principle of virtual work):

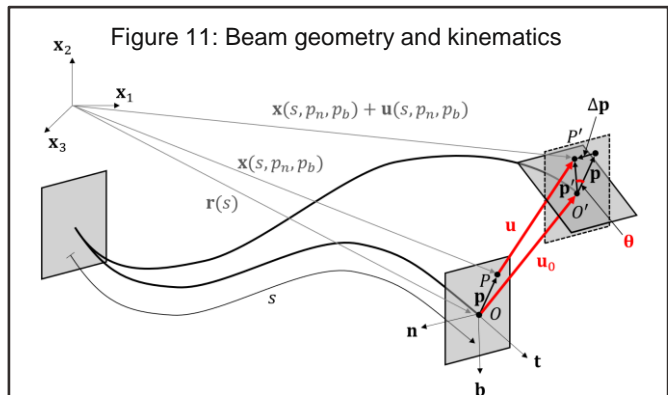
$$\delta W_{\text{int}} = \int_V (\sigma_{tt} \delta \varepsilon_{tt} + \tau_{tn} \delta \gamma_{tn} + \tau_{tb} \delta \gamma_{tb}) dV \quad \frac{dV}{J} = J dA ds, \quad J \text{ is the determinant of } \mathbf{J}, \quad J = 1 - kp_n$$

$$\delta W_{\text{ext}} = \int_l (q_t \delta u_{0t} + q_n \delta u_{0n} + q_b \delta u_{0b} + m_t \delta \theta_t + m_n \delta \theta_n + m_b \delta \theta_b) ds$$

$$\delta W_{\text{int}} = \delta W_{\text{ext}} \Rightarrow$$

Sectional stress resultants  $N = \int_A \sigma_{tt} dA, Q_n = \int_A \tau_{tn} dA, \dots$

$\left( \frac{dN}{ds} - \kappa Q_n \right) + q_t = 0$	$\left( \frac{dM_t}{ds} - \kappa M_n \right) + m_t = 0$
$\left( \kappa N + \frac{dQ_n}{ds} - \tau Q_b \right) + q_n = 0$	$\left( \kappa M_t + \frac{dM_n}{ds} - \tau M_b \right) - Q_b + m_n = 0$
$\left( \tau Q_N + \frac{dQ_b}{ds} \right) + q_b = 0$	$\left( \tau M_n + \frac{dM_b}{ds} \right) + Q_n + m_b = 0$



Beam axis is represented by a parametric curve  $\mathbf{r}(s)$

The Frenet-Serret local system of reference:

$$\mathbf{t}(s) = \frac{d\mathbf{r}(s)/ds}{\|d\mathbf{r}(s)/ds\|}, \quad \mathbf{n}(s) = \frac{d^2\mathbf{r}(s)/ds^2}{\|d^2\mathbf{r}(s)/ds^2\|}; \quad \mathbf{b}(s) = \mathbf{t} \times \mathbf{n}$$

The Frenet-Serret formula:

$$\begin{bmatrix} \frac{d\mathbf{t}}{ds} \\ \frac{d\mathbf{n}}{ds} \\ \frac{d\mathbf{b}}{ds} \end{bmatrix} = \begin{bmatrix} 0 & \kappa & 0 \\ -\kappa & 0 & \tau \\ 0 & -\tau & 0 \end{bmatrix} \begin{bmatrix} \mathbf{t} \\ \mathbf{n} \\ \mathbf{b} \end{bmatrix}$$

Curvature  $\kappa$ :  
 $\kappa(s) = \|d^2\mathbf{r}(s)/ds^2\|$

Torsion  $\tau$ :  
 $\tau(s) = d\mathbf{n}(s)/ds \cdot \mathbf{b}$

$\mathbf{u}_0$  – displacement at reference point  $O$

$\theta$  – rotation of the cross-section

$\mathbf{p}$  – position vector of point  $P$  on the section

[5] Ref: Yin, H., Lale, E., and Cusatis, G. "Generalized Formulation for the Behavior of Geometrically Curved and Twisted Three-Dimensional Timoshenko Beams and Its Isogeometric Analysis Implementation." ASME. J. Appl. Mech. July 2022; 89(7): 071003.

# Isogeometric beam lattice: element verifications

- Linear elastic behaviors of the beam element: static responses [5].

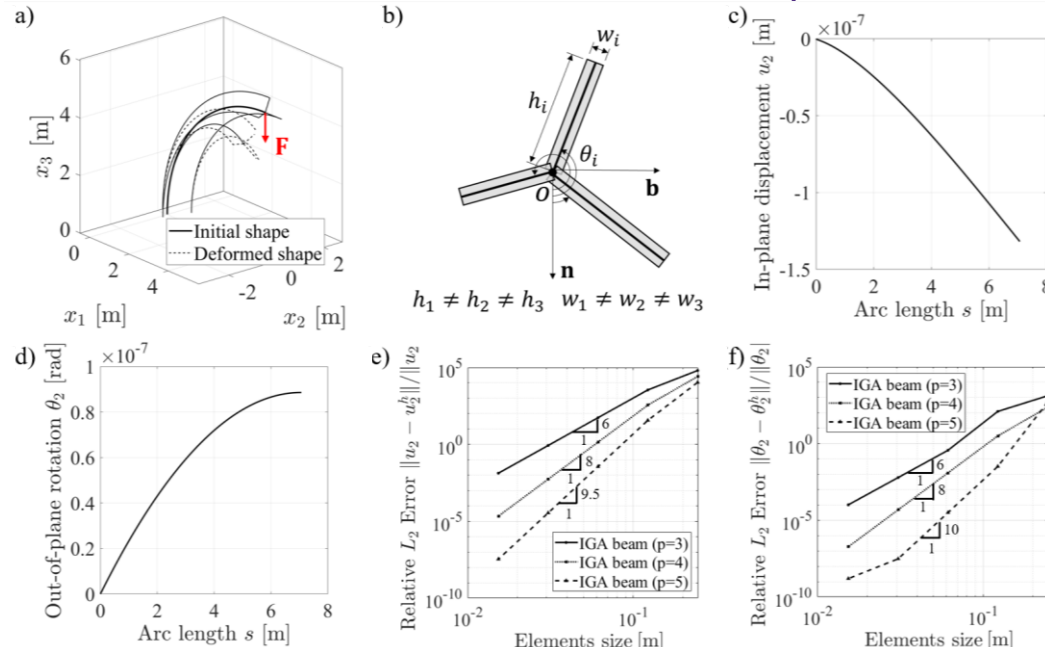


Figure 12: IGA beam verification, tip loaded curved beam with a cruciform cross-section: a) initial shape and the deformed shape in 3D, b) cruciform cross section of the beam, c) and d) displacement  $u_2$  and rotation  $\theta_2$  v.s. the arc-length  $s$ , e) and f) convergence studies of displacement  $u_2$  and rotation  $\theta_2$

[5] Ref: Yin, H., Lale, E., and Cusatis, G. "Generalized Formulation for the Behavior of Geometrically Curved and Twisted Three-Dimensional Timoshenko Beams and Its Isogeometric Analysis Implementation." ASME. J. Appl. Mech. July 2022; 89(7): 071003.

# Connector

- 1D connection elements, named *connectors* have been formulated. They transversely connect pairs of adjacent beams, and account for the in-plane deformability of the cell walls.

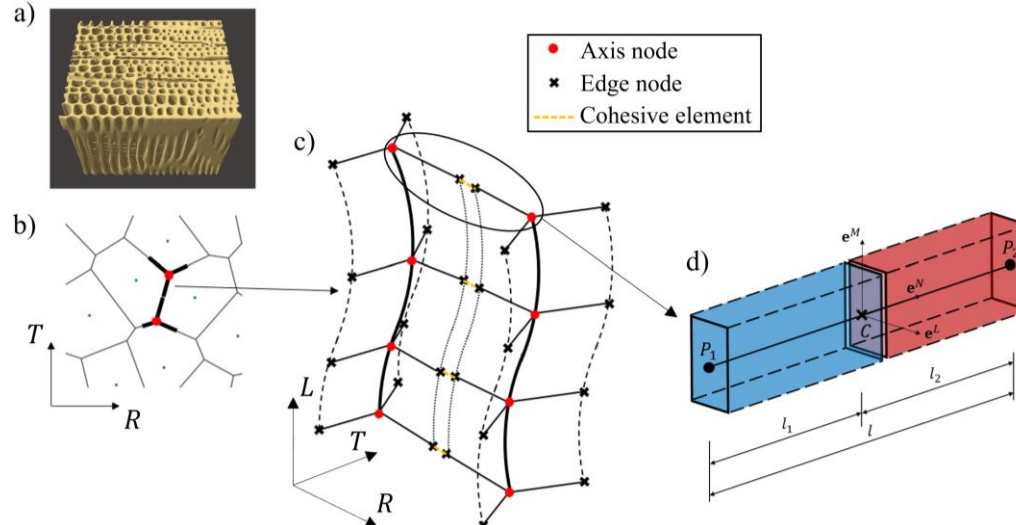


Figure 13: a) 3D tomographic model of wood mesostructure , b) RT plane view of wood lattices, c) 3D view of wood lattices, and d) conceptual diagram of the transverse connector

# Connector

- The formulation of the connectors was derived by allowing discontinuities in displacement and based on the cohesive fracture laws for quasi-brittle materials.

Kinematics:

$$\mathbf{u}_{ci} = \mathbf{u}_I + \boldsymbol{\theta}_I \times (\mathbf{x}_c - \mathbf{x}_I) \quad I \in 1,2$$

$$[\![\mathbf{u}_c]\!] = \mathbf{u}_{c2} - \mathbf{u}_{c1}$$

Displacement jump

$$\varepsilon_N = \mathbf{e}^N \cdot [\![\mathbf{u}_c]\!]/l \quad \varepsilon_M = \mathbf{e}^M \cdot [\![\mathbf{u}_c]\!]/l \quad \varepsilon_L = \mathbf{e}^L \cdot [\![\mathbf{u}_c]\!]/l$$

$E_0$  – mesoscale normal modulus  
 $\alpha$  – normal-shear coupling ratio  
 $\sigma_t$  – tensile strength  
 $G_t$  – tensile fracture energy  
 $r_{st}$  – shear-normal strength ratio

Equilibrium is enforced through the principle of virtual work.

For the axial behavior ( $\varepsilon_N$ -  $\sigma_N$ ), constitutive laws:  $\dot{\sigma} = E_0 \dot{\varepsilon} \quad 0 \leq \sigma \leq \sigma_{bt}$

where effective stress  $\sigma = \sqrt{\sigma_N^2 + \sigma_T^2/\alpha}$ ,  $\sigma_T = \sqrt{\sigma_M^2 + \sigma_L^2}$

effective strain  $\varepsilon = \sqrt{\varepsilon_N^2 + \alpha \varepsilon_T^2}$ ,  $\varepsilon_T = \sqrt{\varepsilon_M^2 + \varepsilon_L^2}$

Effective stress boundary  $\sigma_{bt} = \sigma_0 \exp(-H_0(\varepsilon - \varepsilon_0)/\sigma_0)$

Strength limit of eff. stress  $\sigma_0 = \sigma_0(\sigma_t, r_{st}, \alpha, \omega)$

Softening modulus  $H_0 = H_t \left( \frac{2\omega}{\pi} \right)^{0.2}$

Direction of straining  $\omega$ :  $\tan \omega = \frac{\varepsilon_N}{\sqrt{\alpha} \varepsilon_T}$

Softening modulus for pure tension  $H_t = 2E_0/(l_t/l - 1)$

Characteristic length  $l_t = 2E_0 G_t / \sigma_t^2$

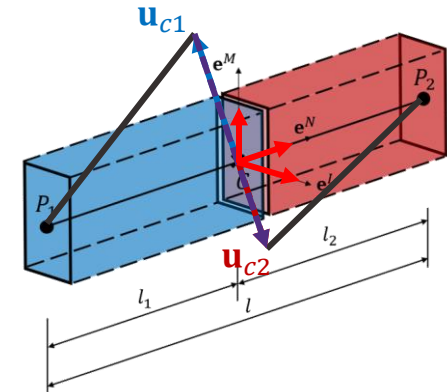


Figure 15: Connector geometry and kinematics

# Connector

For the tangential behaviors ( $\varepsilon_M - \sigma_M$  and  $\varepsilon_L - \sigma_L$ ), constitutive laws:

$$\dot{\sigma}_M = \alpha E_0 (\dot{\varepsilon}_M - \dot{\varepsilon}_M^p) \quad \dot{\sigma}_L = \alpha E_0 (\dot{\varepsilon}_L - \dot{\varepsilon}_L^p)$$

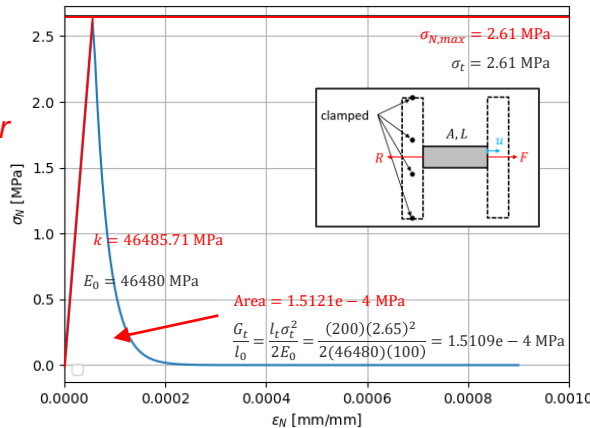
$$\dot{\varepsilon}_M^p = \lambda \frac{\partial \varphi}{\partial \sigma_M} \quad \dot{\varepsilon}_L^p = \lambda \frac{\partial \varphi}{\partial \sigma_L}$$

Plastic Potential  $\varphi = \sigma_T - \sigma_{bs}$

The shear stress boundary  $\sigma_{bs} = r_{st}\sigma_t + (\mu_0 - \mu_\infty)\sigma_{N0} - \mu_\infty\sigma_N - (\mu_0 - \mu_\infty)\sigma_{N0}\exp(\sigma_N/\sigma_{N0})$

$E_0$  – mesoscale normal modulus  
 $\alpha$  – normal-shear coupling ratio  
 $r_{st}$  – shear-normal strength ratio  
 $\mu_0$  – initial frictional slope  
 $\mu_\infty$  – asymptotic frictional slope  
 $\sigma_{N0}$  – transitional normal stress

Normal behavior



Shear behavior

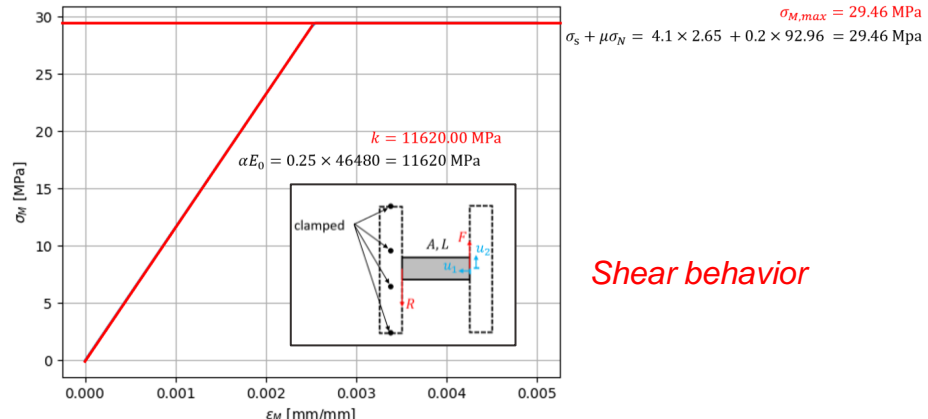


Figure 16: Connector verifications: a) axial (N) behavior, softening, and b) tangential (M or L) behavior, frictional effect

# Connector: longitudinal direction

- Longitudinal connectors have been formed to permit the simulation of **fiber rupture**. They share the same cross-sectional properties with the associated beam elements.

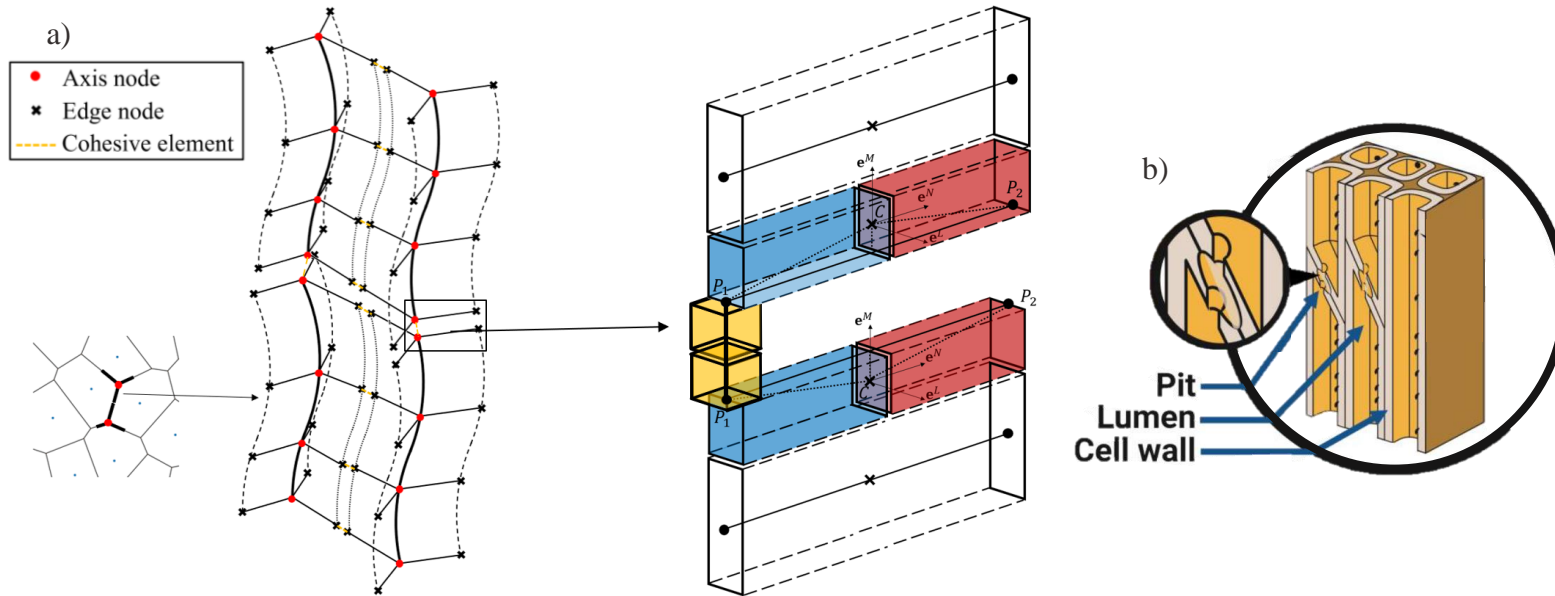


Figure 14: a) Conceptual diagram of the longitudinal connector, b) weak joints in microstructure of wood (modified from [6])

# Elastic orthotropy

- The macroscopic elastic properties of spruce wood specimens were investigated with the *CBL model*. The material orthotropy was correctly simulated, notice that the in-plane anisotropy was only from the mesoscale geometry of spruce wood.

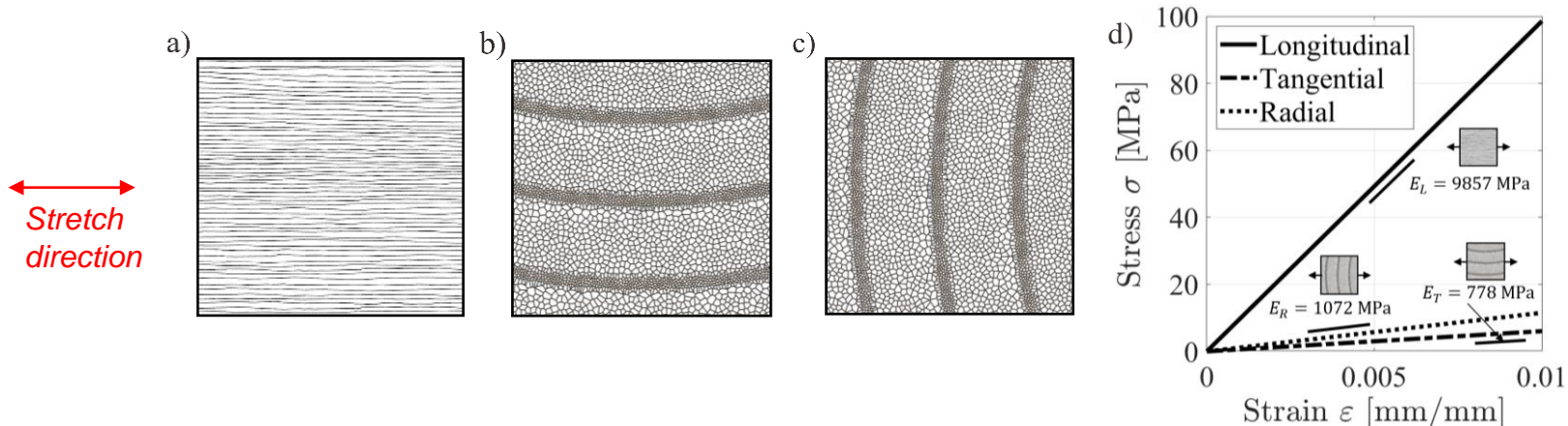
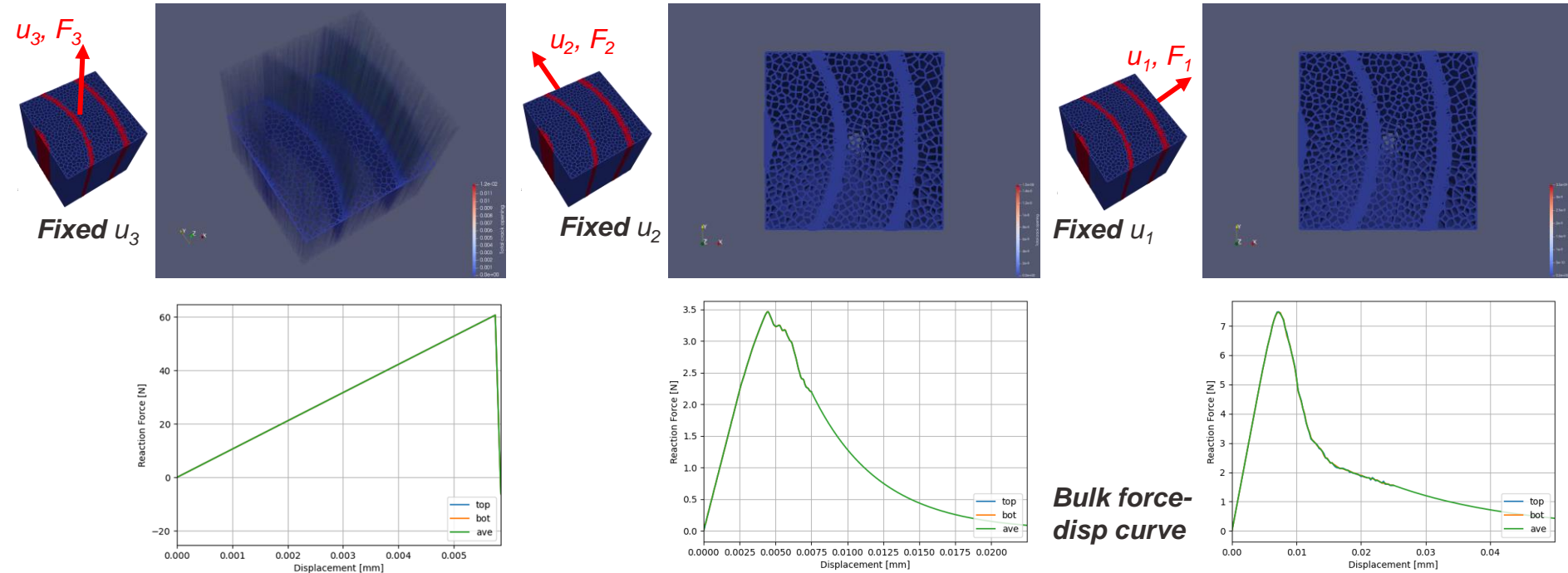


Figure 17: Elastic orthotropy of wood, lateral view of: a) L-uniaxial tension test specimen, b) T-tension test specimen, c) R-tension test specimen, and d) simulated results

# Fracture

- The CBL model can be used for the simulation of nonlinear behaviors of wood, e.g., fracture. The calibration of parameters and the modification of the formulation are ongoing.



# Fracture

- The *CBL model* can be used for the simulation of nonlinear behaviors of wood, e.g., fracture. The calibration of parameters and the modification of the formulation are ongoing.

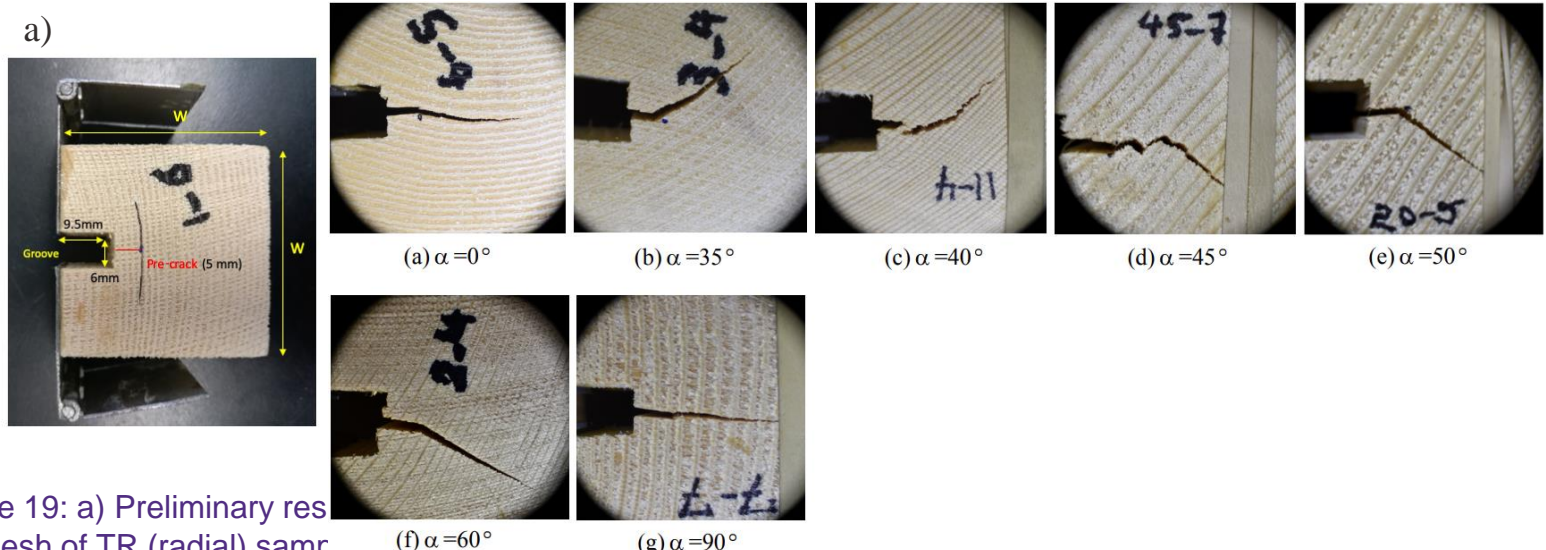


Figure 10. Crack growth path at different angles.

[7] Ref: Belalpour Dastjerdi, Parinaz, and Eric N. Landis. "Growth Ring Orientation Effects in Transverse Softwood Fracture." Materials 14.19 (2021): 5755.

# Conclusions and Future Work

- A 3D Connector-Beam Lattice (CBL) Model has been formulated to capture the cellular morphology and the material heterogeneity at mesoscale of wood.
- The macroscopic orthotropic elasticity of wood was correctly simulated with the model.
- The distinct fracturing behaviors in different directions of the notched tension tests of wood were captured.
- The formulation of the Beam Lattice Model will be further developed to incorporate more nonlinear behaviors (e.g., finite deformation, cell wall buckling) and multiphysics analyses (e.g., thermo-hygral induced warping) of engineered wood products.

# Thank you!



*RingsPy*  
*Github repo*



*Cusatis group*  
*website*



Northwestern | McCORMICK SCHOOL OF  
ENGINEERING



# Wood mesh generation: wood cells

- Non-overlapped cell points (sites) with radii corresponding to the cell sizes are randomly placed in the annual rings structure, a 2D Voronoi mesh is then generated.

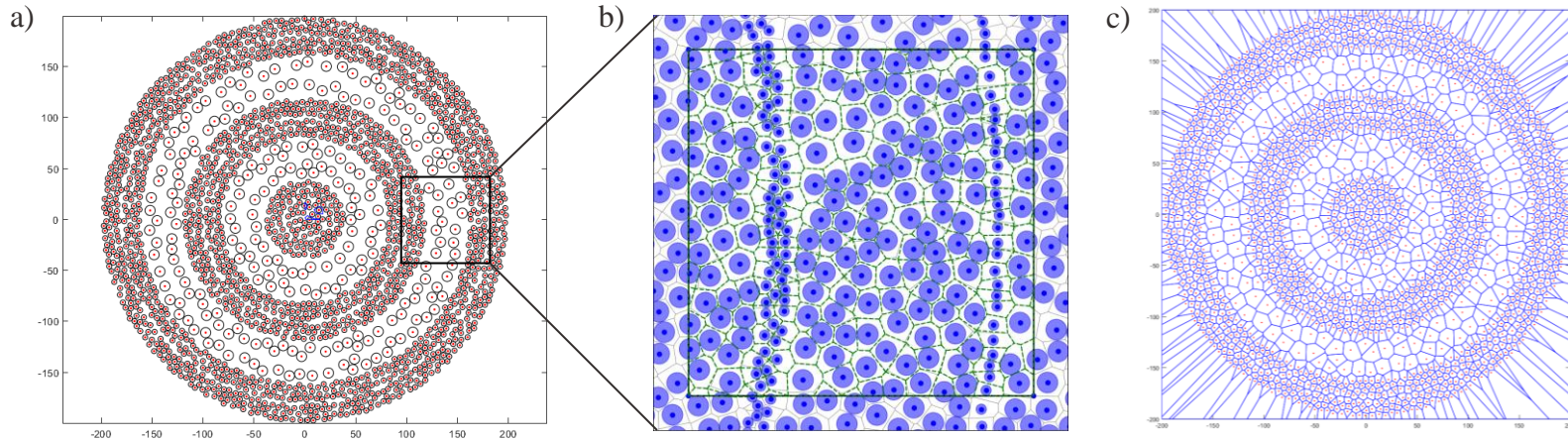


Figure 8: a) Random circle placement in the annual rings structure, b) Voronoi tessellation of the wood sites, and c) the corresponding 2D Voronoi mesh of a)

# Isogeometric beam lattice

- The formulation of the beam lattice was derived.

The full list of sectional stress resultants:

$$N = \int_A \sigma_{tt} dA \quad Q_n = \int_A \tau_{tn} dA \quad Q_b = \int_A \tau_{tb} dA$$

$$M_t = \int_A (\tau_{tb} p_n - \tau_{tn} p_b) dA \quad M_n = \int_A \sigma_{tt} p_b dA \quad M_b = - \int_A \sigma_{tt} p_n dA$$

For linear elastic beam behavior:

$$\sigma_{tt} = E_b \varepsilon_{tt} \quad \tau_{tn} = G_b \gamma_{tn} \quad \tau_{tb} = G_b \gamma_{tb}$$

$E_b$  – beam elastic modulus  
 $G_b$  – beam shear modulus

Introduce the equivalent sectional properties:

$$A^* = \int_A \frac{1}{1 - \kappa p_n} dA \quad A_n^* = \alpha_n A^* \quad A_b^* = \alpha_b A^*$$

$$S_n^* = \int_A \frac{p_b}{1 - \kappa p_n} dA \quad S_b^* = \int_A \frac{p_n}{1 - \kappa p_n} dA \quad I_{tt}^* = \int_A \frac{p_n^2 + p_b^2}{1 - \kappa p_n} dA$$

$$I_{nn}^* = \int_A \frac{p_b^2}{1 - \kappa p_n} dA \quad I_{bb}^* = \int_A \frac{p_n^2}{1 - \kappa p_n} dA \quad I_{nb}^* = \int_A \frac{p_n p_b}{1 - \kappa p_n} dA$$

$J = 1 - \kappa p_n$  represents the influence of beam curvature

$$\begin{aligned} \left( \frac{dN}{ds} - \kappa Q_n \right) + q_t &= 0 & \left( \frac{dM_t}{ds} - \kappa M_n \right) + m_t &= 0 \\ \left( \kappa N + \frac{dQ_n}{ds} - \tau Q_b \right) + q_n &= 0 & \left( \kappa M_t + \frac{dM_n}{ds} - \tau M_b \right) - Q_b + m_n &= 0 \\ \left( \tau Q_N + \frac{dQ_b}{ds} \right) + q_b &= 0 & \left( \tau M_n + \frac{dM_b}{ds} \right) + Q_n + m_b &= 0 \end{aligned}$$

Recall the definitions of the generalized sectional strains  $\boldsymbol{\varepsilon}_0$  and sectional flexural strains  $\boldsymbol{\chi}$ :

$$\boldsymbol{\varepsilon} = \frac{1}{J} (\boldsymbol{\varepsilon}_0 + \boldsymbol{\chi} \times \mathbf{p}) \quad \text{where } \boldsymbol{\varepsilon}_0 = \frac{d\mathbf{u}_0}{ds} - \boldsymbol{\theta} \times \mathbf{t}$$

vector  $\boldsymbol{\varepsilon} = [\varepsilon_{tt} \quad \gamma_{tn} \quad \gamma_{tb}]^T$ , not tensor  $\boldsymbol{\epsilon}$

$$\boldsymbol{\chi} = \frac{d\boldsymbol{\theta}}{ds}$$

The elastic behavior can be written as:

$$\begin{bmatrix} N \\ Q_n \\ Q_b \\ M_t \\ M_n \\ M_b \end{bmatrix} = \begin{bmatrix} EA^* & 0 & 0 & 0 & ES_n^* & -ES_b^* \\ 0 & GA_n^* & 0 & -GS_n^* & 0 & 0 \\ 0 & 0 & GA_b^* & GS_b^* & 0 & 0 \\ 0 & -GS_n^* & GS_b^* & GI_{tt}^* & 0 & 0 \\ ES_n^* & 0 & 0 & 0 & EI_{nn}^* & -EI_{nb}^* \\ -ES_b^* & 0 & 0 & 0 & -EI_{nb}^* & EI_{bb}^* \end{bmatrix} \begin{bmatrix} \varepsilon_{0tt} \\ \varepsilon_{0nn} \\ \varepsilon_{0bb} \\ \boldsymbol{\chi}_t \\ \boldsymbol{\chi}_n \\ \boldsymbol{\chi}_b \end{bmatrix}$$

# Isogeometric beam lattice

- Isogeometric analysis (IGA) technique, popularized by Hughes et al. in 2005 [5], was used to accurately represent the geometry, and to alleviate the shear locking of curved beams during the analysis.

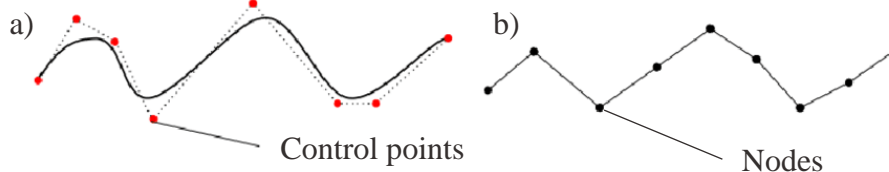


Figure 11: a) IGA mesh (NURBS geometry), b) FEM mesh (Lagrange geometry)

- The IGA uses Non-Uniform Rational B-Splines (NURBS), which are originally used to represent the geometry in CAD industry, as shape functions to interpolate also the solution fields. Essentially, it is still a finite element method.

$$\mathbf{u} = \sum_{I=1}^{N_{cp}} R_I \mathbf{u}_I^e \quad \boldsymbol{\theta} = \sum_{I=1}^{N_{cp}} R_I \boldsymbol{\theta}_I^e$$

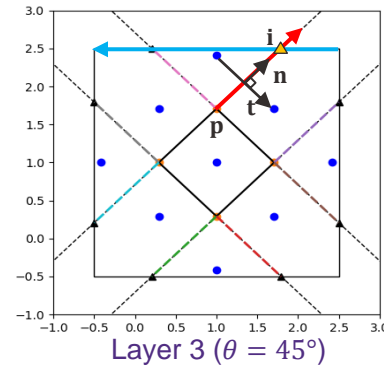
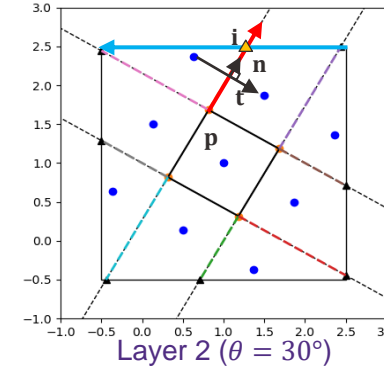
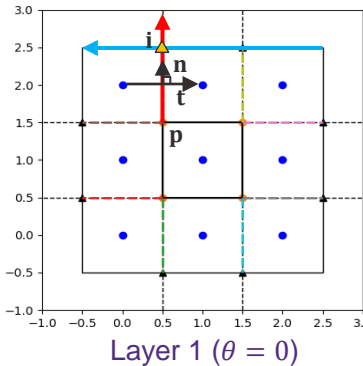
where  $N_{cp}$  is the number of control points supported by one element,  $R_I$  are the NURBS shape functions,  $\mathbf{u}_I^e$  is the nodal displacement vector,  $\boldsymbol{\theta}_I^e$  is the nodal rotation vector.

[5] Ref: Hughes, Thomas JR, John A. Cottrell, and Yuri Bazilevs. "Isogeometric analysis: CAD, finite elements, NURBS, exact geometry and mesh refinement." *Computer methods in applied mechanics and engineering* 194.39-41 (2005): 4135-4195.

# Wood Mesh Generator

## The boundary cutting algorithm

1. Create a bounding box (line segments)
2. Find infinite Voronoi ridges and find the finite end (vertex)  $p$  of the infinite ridge
3. Store the information for each infinite Voronoi ridge (finite end vertex, corresponding site points)
4. Find the intersection point  $i$  of the infinite Voronoi ridge and the boundary line segments using the “*intersection*” algorithm
5. Replace the infinite ridge to finite ridge with two end vertices:  $p$  and the intersection point  $i$
6. For the next layer, repeat step 4 and 5 to find new intersection points and new finite ridges



# Beam Lattice Model: potential failure position of cells

- The connector element by now only assumes one potential failure position, which is the center of the connector (joint of beam fringes).
- From the macroscopic point of view, this assumption is acceptable for describing the **cell wall fracture and failure** (low resolution of cracks).
- However, for some micro-failure mechanisms of wood, e.g., **fiber delamination**, the two ends should also be considered as potential failure positions.

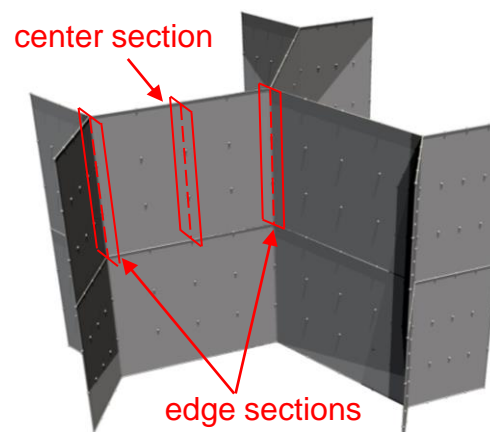
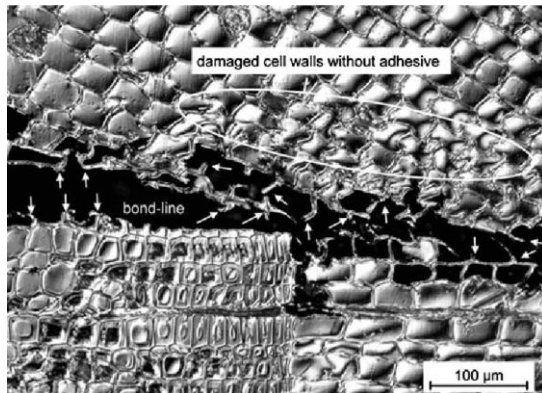
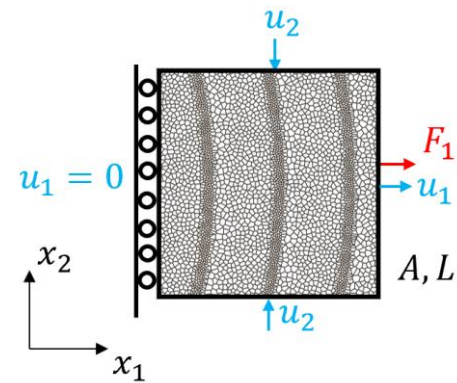
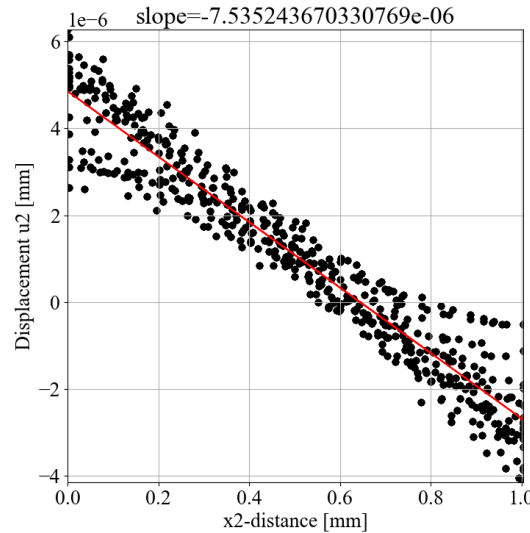
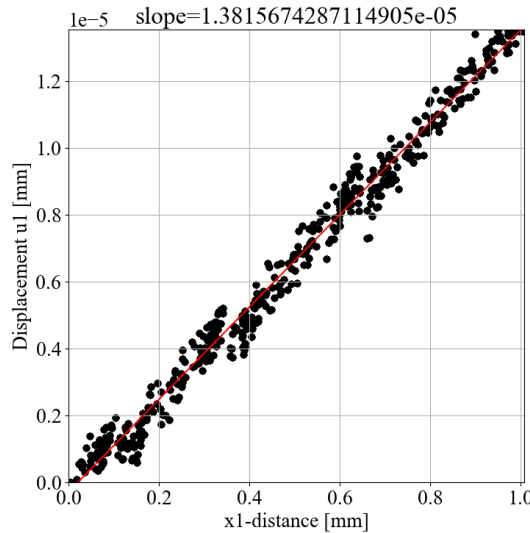


Image: Bucur, V. and Martin, P.A., 2011. Delamination in wood, wood products and wood-based composites (p. 402). Springer.

# Beam Lattice Model: simulating the Poisson effect

Poisson effects of the beams: tension in Radial (R) direction, alpha = 0.0625

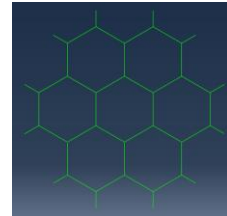
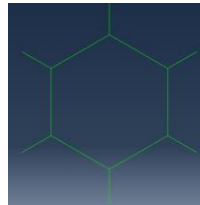
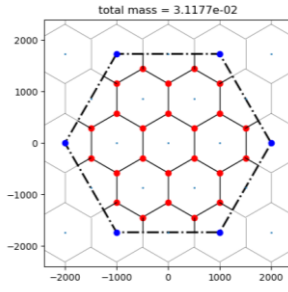
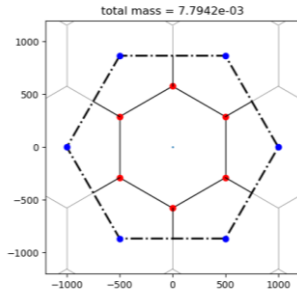


$$\alpha = 0.0625 \Leftrightarrow \nu_{12} = 0.545$$

$\nu_{ij}$  - Poisson's ratio that corresponds to a contraction in  $j$  when an extension is applied in  $i$

# Beam Lattice Model: simulating the Poisson effect

- The Poisson effect is typically simulated by changing the parameter  $\alpha$ . By reducing  $\alpha$ , a discrete assembly of lattices exhibits a larger macroscopic Poisson's ratio.
- The *spectral stiffness method* for the Beam Lattice Model is under development in order to find the best fit for direction dependent elastic constants.



Macroscopic eigenstresses & eigenstrains :  $\vec{\sigma}_1 = \underline{E}_1 \vec{\epsilon}$      $\vec{\epsilon}_1 = \lambda_1^{-1} \vec{\sigma}_1 = \lambda_1^{-1} \underline{E}_1 \vec{\sigma}$   
 microplane eigenstresses & eigenstrains :

$$\begin{aligned}\vec{\sigma}_{c1} &= P_c \vec{\sigma}_1 \Rightarrow \vec{\sigma}_{c1} = P_c \underline{E}_1 \vec{\sigma} \\ \vec{\epsilon}_{c1} &= \underline{E}_c^{-1} \vec{\sigma}_{c1} = \underline{E}_c^{-1} P_c \underline{E}_1 \vec{\sigma} \\ \underline{E}_c^{-1} &= \begin{bmatrix} \frac{1}{E_0} & 0 & 0 \\ 0 & -\frac{1}{\alpha E_0} & 0 \\ 0 & 0 & \frac{1}{\alpha E_0} \end{bmatrix}\end{aligned}$$

$$\underline{E}_c^{-1}$$

In a control volume  $\Omega$ , the total strain energy

$$U_{1,\text{micro}} = \frac{1}{2} \sum_{c \in \Omega} V_c \vec{\epsilon}_{c1}^T \vec{\sigma}_{c1} = \frac{1}{2} \sum_{c \in \Omega} V_c \vec{\sigma}^T (\underline{E}_1^T P_c^T \underline{E}_c^{-1} P_c \underline{E}_1) \vec{\sigma}$$

$$U_{1,\text{macro}} = \frac{1}{2} V_\Omega \vec{\epsilon}^T \vec{\sigma} = \frac{1}{2} V_\Omega \vec{\sigma}^T (\underline{E}_1^T \lambda_1^{-1} \underline{E}_1) \vec{\sigma}$$

the PVW :  $U_{1,\text{micro}} = U_{1,\text{macro}} \Rightarrow$

$$\sum_{c \in \Omega} V_c (\underline{E}_1^T P_c^T \underline{E}_c^{-1} P_c \underline{E}_1) = V_\Omega (\underline{E}_1^T \lambda_1^{-1} \underline{E}_1)$$

# Beam Lattice Model: Explicit dynamics formulation

No need for globalization

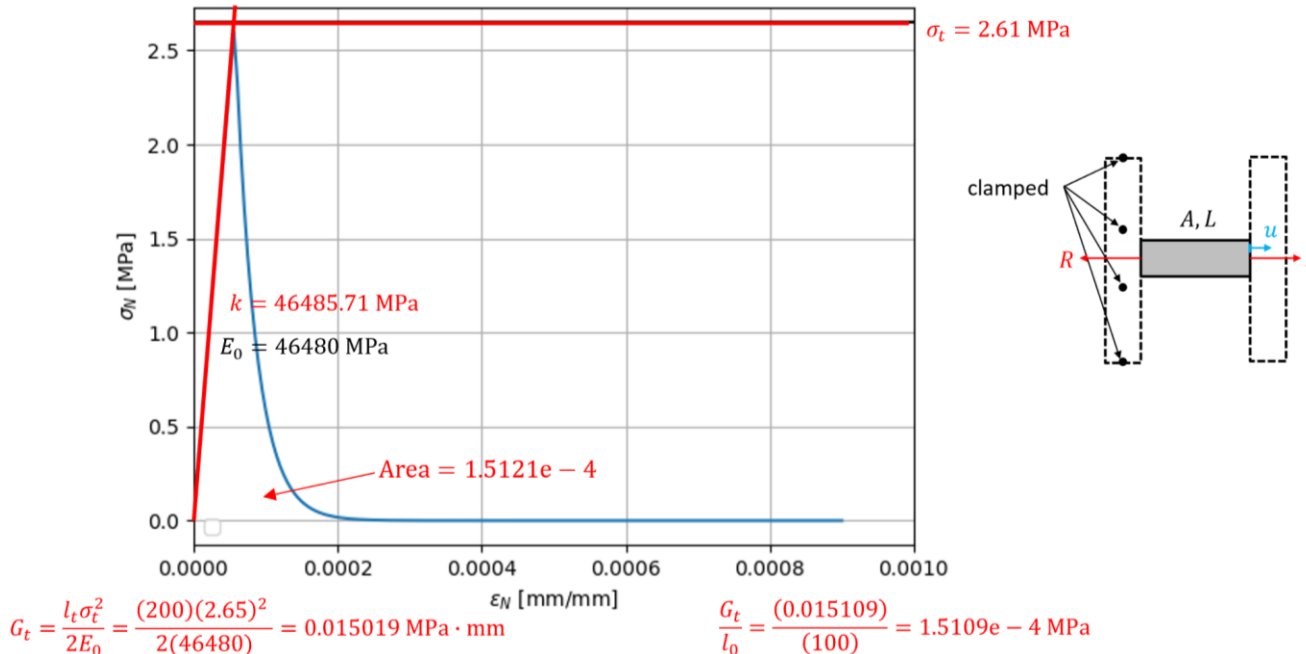
$$\mathbf{M} = \begin{bmatrix} \mathbf{I} & \mathbf{0} \\ \mathbf{0} & \mathbf{T} \end{bmatrix}^T \begin{bmatrix} \mathbf{N} & \mathbf{0} \\ \mathbf{0} & \mathbf{N} \end{bmatrix}^T \begin{bmatrix} \rho A^* & 0 & 0 & 0 & \rho S_n^* & -\rho S_b^* \\ 0 & \rho A^* & 0 & -\rho S_n^* & 0 & 0 \\ 0 & 0 & \rho A^* & \rho S_b^* & 0 & 0 \\ 0 & -\rho S_n^* & \rho S_b^* & \rho I_t^* & 0 & 0 \\ \rho S_n^* & 0 & 0 & 0 & \rho I_{nn}^* & -\rho I_{nb}^* \\ -\rho S_b^* & 0 & 0 & 0 & -\rho I_{nb}^* & \rho I_{bb}^* \end{bmatrix} \begin{bmatrix} \mathbf{N} & \mathbf{0} \\ \mathbf{0} & \mathbf{N} \end{bmatrix} \begin{bmatrix} \mathbf{I} & \mathbf{0} \\ \mathbf{0} & \mathbf{T} \end{bmatrix}$$

- The mass matrix in explicit analysis requires diagonal lumping for the easy inversion  
→ **no coupling (off-diagonal) entries** → appropriate lumping is needed

$$\mathbf{M} = \begin{bmatrix} \mathbf{I} & \mathbf{0} \\ \mathbf{0} & \mathbf{T} \end{bmatrix}^T \begin{bmatrix} \mathbf{N} & \mathbf{0} \\ \mathbf{0} & \mathbf{N} \end{bmatrix}^T \begin{bmatrix} \rho A^* & 0 & 0 & 0 & 0 & 0 \\ 0 & \rho A^* & 0 & 0 & 0 & 0 \\ 0 & 0 & \rho A^* & 0 & 0 & 0 \\ 0 & 0 & 0 & \rho I_t^* & 0 & 0 \\ 0 & 0 & 0 & 0 & \rho I_{nn}^* & 0 \\ 0 & 0 & 0 & 0 & 0 & \rho I_{bb}^* \end{bmatrix} \begin{bmatrix} \mathbf{N} & \mathbf{0} \\ \mathbf{0} & \mathbf{N} \end{bmatrix} \begin{bmatrix} \mathbf{I} & \mathbf{0} \\ \mathbf{0} & \mathbf{T} \end{bmatrix}$$

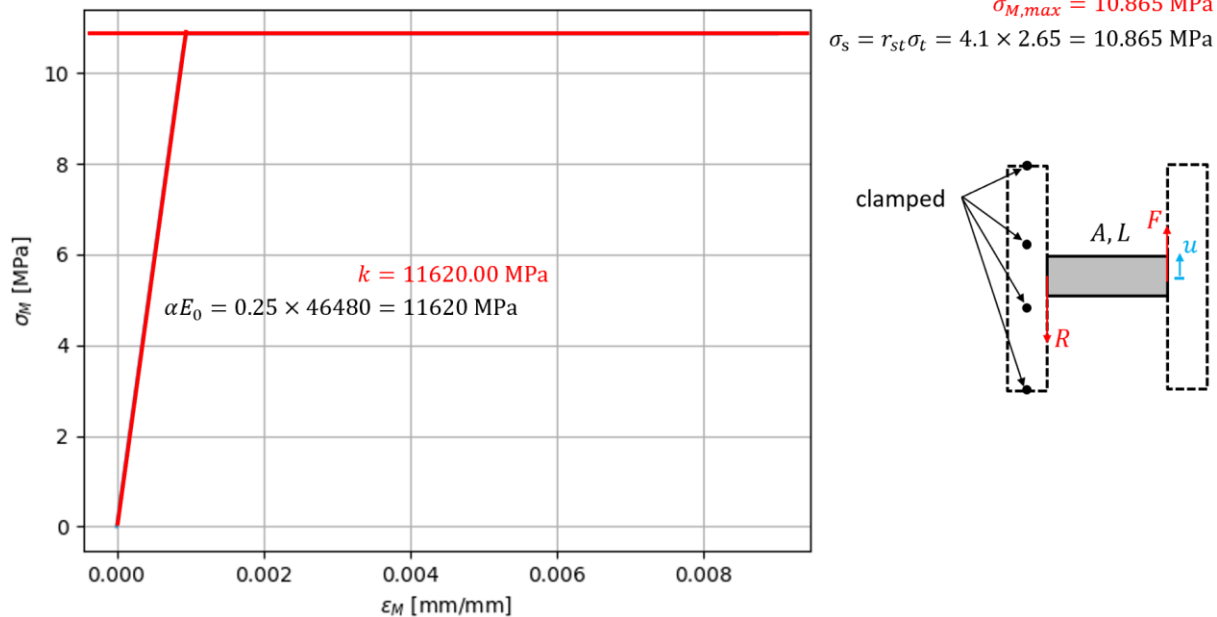
# Beam Lattice Model: Element verifications

- Nonlinear behaviors of the connector: tension in axial (N) direction



# Beam Lattice Model: Element verifications

- Nonlinear behaviors of the connector: pure shear in tangential (M) direction



# Beam Lattice Model: Element verifications

- Nonlinear behaviors of the connector: confined shear in tangential (M) direction

